Electronic Supplementary Information

A colossal barocaloric effect induced by the creation of a high-pressure phase

Zhao Zhang, Xiaoming Jiang, Takanori Hattori, Xiong Xu, Min Li, Chenyang Yu, Zhe Zhang, Dehong Yu, Richard Mole, Shin-ichiro Yano, Jie Chen, Lunhua He, Chin-Wei Wang, Hui Wang,* Bing Li* and Zhidong Zhang

Experiment methods

Polycrystalline KPF_6 powder (99.98%), which was purchased from Aladdin, was checked using an X-ray diffractometer (D8 Advance, Bruker) and a differential scanning calorimeter (DSC) (Q1000, TA Instruments).

The KPF_6 powder was pelletized and put in high-pressure Hastelloy cells. The heat flow data were collected using the DSC (µDSC 7 EVO, Setaram) under 0.1, 15, 20, 25, 30, 35, 40, 45, 50, 55, 60, 70, 80 and 90 MPa. The details have been published elsewhere.[1-4] The single-crystal X-ray diffraction experiments were performed on a Pilatus CCD diffractometer equipped with graphite-monochromated Mo-K_α radiation (λ = 0.71073 Å) at 300 K and 250 K. All data were processed by using Jana2006.[5] Temperature-variable XRD patterns were collected by using a Rigaku Smartlab diffractometer with Cu-K_α radiation (λ = 1.5406 Å). The polycrystalline sample was cooled down to 240 K. The measurements were performed at 240, 245, 250, 255, 260, 265, 270, 280, 290 and 300 K after keeping for 20 min. All patterns were analyzed with Le Bail method using the Fullprof_Suite program. [6]

NPD experiments were performed on the polycrystalline KPF_6 powder at general purpose powder diffractometer (GPPD) of China Spallation Neutron Source (CSNS) in Dongguan, China.[7] The powder was loaded into a vanadium can (ϕ = 9 mm, L = 70 mm) and the NPD pattern was collected with wavelength ranging from 0.1 Å to 4.9 Å under vacuum at 240 and 300 K. And a constant-temperature scan was collected for 2 h. The Le Bail method was used to analyze crystal structures by the Fullprof_Suite program.[6]

Pressure-dependent NPD experiments were performed on the polycrystalline KPF_6 powder at the powder diffractometer, which specializes in high-pressure experiments,

BL11 PLANET of J-PARC in Japan.[8] In the experiments, we used a piston cylinder cell made of CuBe. The powder was put in a Teflon cell together with a pressure transmitting medium of Fluorinert (3M, FC72). Two pieces of Pb plates were placed at the bottom in the cell as a pressure marker.[9] The sample is compressed to a targeted load based on the pressure-load curves determined beforehand. The generated pressure during the experiment was determined from the lattice parameter of Pb based on its equation of state. The high-pressure cell was attached to the 4 K GM refrigerator (CryoMini, Iwatani). The temperature of the sample was measured by a resistance temperature sensor (Cernox, Lakeshore) attached to the adapter connecting the high-pressure cell to the cold head. The temperature difference between the sample and the sensor was checked in advance and found to be less than 0.1 K. The diffraction patterns were collected at P-T points of $P \approx$ 0.1, 0.3, 0.8 GPa and T = 255, 297 K. To check the lower-pressure structures, several short scans were performed under 100 MPa. The Le Bail method was used to analyze crystal structures by the Fullprof_Suite program.[7] The elastic scans were performed on the cold-neutron triple-axis spectrometer SIKA at Australian Center for Neutron Scattering (ACNS) of Australian Nuclear Science and Technology Organisation (ANSTO) in Sydney, Australia.[10] The incident neutron energies E_i and final neutron energies E_f were fixed at 8.0 meV. Constant-Q scans were made around 1.4 Å^{-1} to obtain the incoherent ENS intensities. The INS experiments were performed on the time-of-flight (TOF) spectrometer PELICAN at ACNS of ANSTO in Sydney, Australia.[11,12] The instrument was configured for incident neutron energy of 3.7 meV, with an energy resolution of 0.135 meV at the elastic line. The powder samples of KPF_6 were loaded into an annular aluminum can with a sample thickness of 1 mm. The experiments were performed at 240 K and 300 K for KPF_6. A background spectrum from an empty can was collected under the same conditions as the sample measurements. The instrument resolution function was measured on a standard vanadium can at 300 K. The spectrum of the vanadium standard was also used for detector normalization. All data reduction and manipulation, including background subtraction and detector normalization, were done using the Large Array Manipulation Program (LAMP).[13] The scattering function $S(Q,E)$, which are a function of scattering wave vectors (Q) and energy transfer (E), were measured on energy gain mode over a wide temperature range. And the

scattering function $S(Q,E)$ transformed to a generalized PDOS by the formula (1), where k_B is the Boltzmann constant and T is the temperature,[14]

$$g(E) = \int \frac{E}{Q^2} S(Q,E) \left(1 - e^{-\frac{E}{k_B T}} \right) dQ \#(1)$$

The Raman spectra at various temperatures and various pressures were recorded on the Raman spectroscope (HORIBA LabRAM HR Evolution, HORIBA Jobin Yvon) at a wavelength of 532 nm. For the atmospheric pressure experiments, we pressed KPF_6 from powder to block. The sample was cooled from 293 K to 233 K, with 10 K as the step, and a constant-temperature scan was carried out for 10 min under ambient pressure. The KPF_6 powder and several standard ruby particles which were used to determine the pressure were put in the diamond anvil cell (DAC) for high-pressure experiments.[3,15,16] The pressure was fixed by screwing on the cell. The pressure-dependent Raman spectra were collected at P-T points of $P = 0.4$, 1.0 GPa and $T = 293$ and 243 K. To achieve the hydrostatic pressure, we use the Si oil as the pressure transmitting medium in the DAC. We fixed the temperature and then varied the pressure for the tests. We tested the Raman spectra at 298 K for 0.1 and 180 MPa; and at 243 K for 0.1 and 100 MPa to determine the phase transition that can occur at low pressure (Fig. S8).

Theoretical calculation method

Density functional theory (DFT) calculations were performed with the Vienna Ab-initio Simulation Package (VASP) as implemented in MedeA.[17] The projector-augmented wave method (PAW)[18] in local density approximation (LDA)[19] form was applied in DFT calculations, and the valence configurations of $4s^1$, $3s^2 3p^3$ and $2s^2 2p^5$ were employed to depict the K, P and F atoms, respectively. The energy cutoff for the plane-wave expansion was 500 eV, and Brillouin zone was sampled adopting the Γ-centered Monkhorst-Pack method[20] with a density of about $2\pi \times 0.03$ Å^{-1}. Calculations were carried out on a 3×3×3 supercell containing 216 atoms to obtain the collective vibrational spectra of phonons by using Phonopy.[21] Structures were optimized with a criterion that the atomic force on each atom becomes weaker than 0.001 eV/Å and the energy convergence is better than 10^{-8} eV. Density functional perturbation theory (DFPT) is a particularly powerful and flexible theoretical technique that allows the

calculation of electron-density linear response within the density functional framework, thereby facilitating the acquisition of vibrational frequencies within crystalline materials.[22] Lattice dynamics calculations were carried out using the Phonopy package,[21] with MedeA-VASP employed as the calculator to obtain interatomic force constants (IFCs) via a DFPT calculation. During post-processing, sampling the phonon frequencies on a 30×30×30 centered q mesh converged the vibrational density of states, and hence the values of thermodynamic properties calculated from it. Raman activity was obtained by computing the macrosocpic dielectric tensor with respect to the mode coordinate along with the phonons at Brillouin zone center.
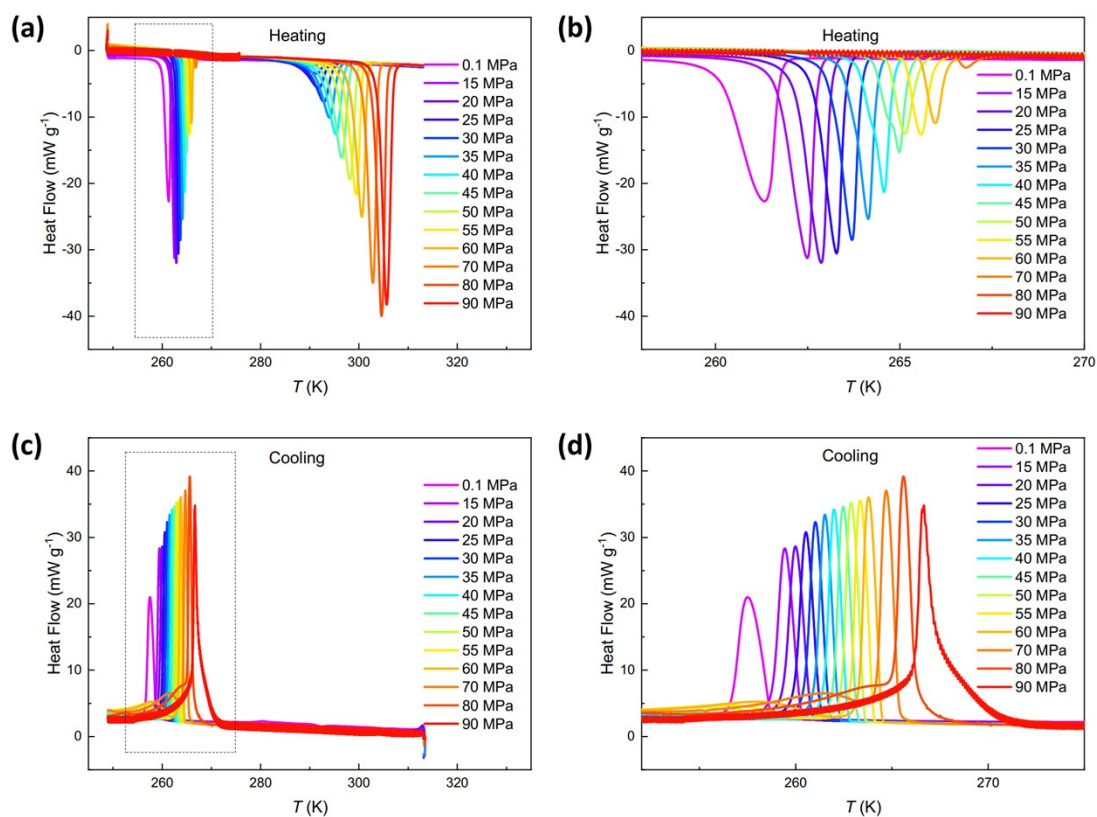
Fig. S1 (a) Pressure-dependent heat flow data at 0.1, 15.0, 20.0, 25.0, 30.0, 35.0, 40.0, 45.0, 50.0, 55.0, 60.0, 70.0, 80.0 and 90.0 MPa on heating from 248 K to 313 K, and (b) is the magnified portion of (a) in the temperature interval between 255 K and 270 K. (c) Pressure-dependent heat flow data at 0.1, 15.0, 20.0, 25.0, 30.0, 35.0, 40.0, 45.0, 50.0, 55.0, 60.0, 70.0, 80.0 and 90.0 MPa on cooling from 313 K to 248 K, and (d) is the magnified portion of (c) in the temperature interval between 252 K and 275 K.
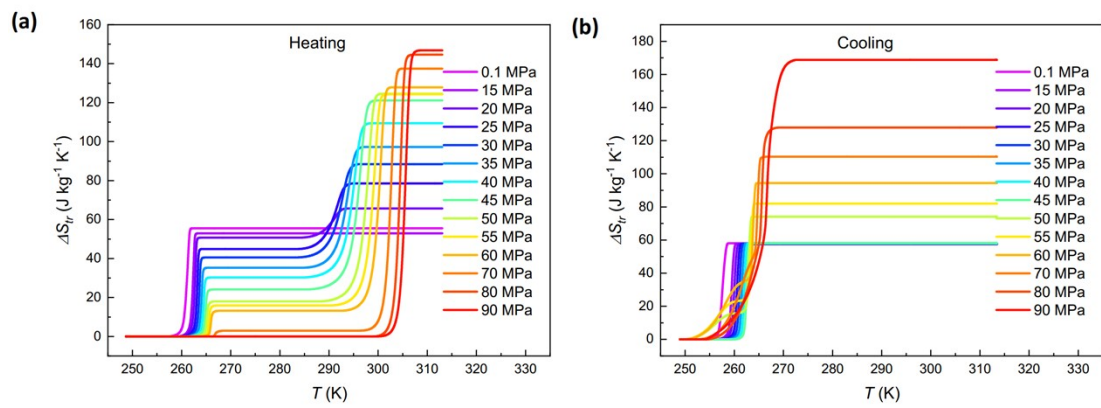
Fig. S2 (a),(b) Pressure-dependent entropy changes (ΔS) at 0.1, 15, 20, 25, 30, 35, 40, 45, 50, 55, 60, 70, 80 and 90 MPa on heating and on cooling, respectively.
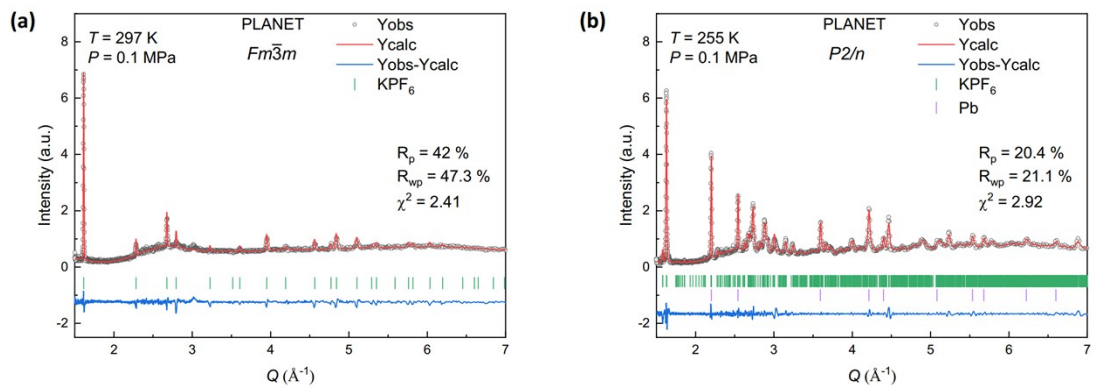
Fig. S3 Pressure-dependent NPD patterns and refinements of KPF_6 at different temperatures. (a) T = 297 K and P = 0.1 MPa; (b) T = 255 K and P = 0.1 MPa;
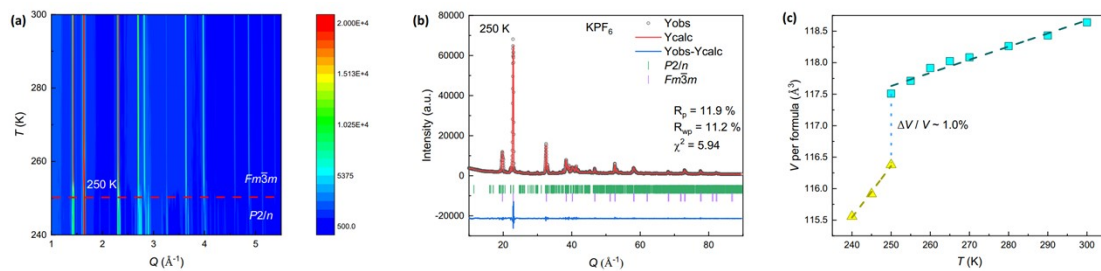
Fig. S4 (a) The contour plot of the XRD patterns in the temperature region from 240 to 300 K. (b) XRD pattern and refinement at 250 K. (c) The variation of the unit cell volume per formula (V) with temperature.
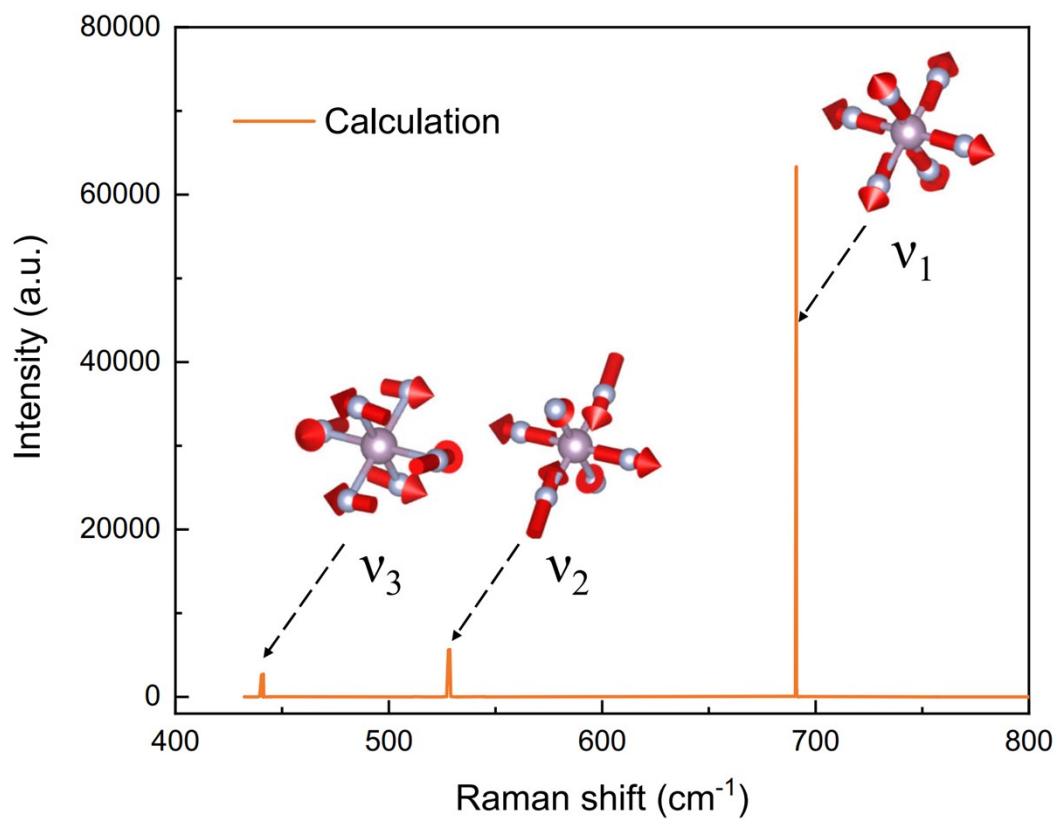
Fig. S5 Calculated Raman spectra of KPF_6 in rhombohedral phase. Insets demonstrate the vibrational modes of PF_6^- ion corresponding to the three peaks.
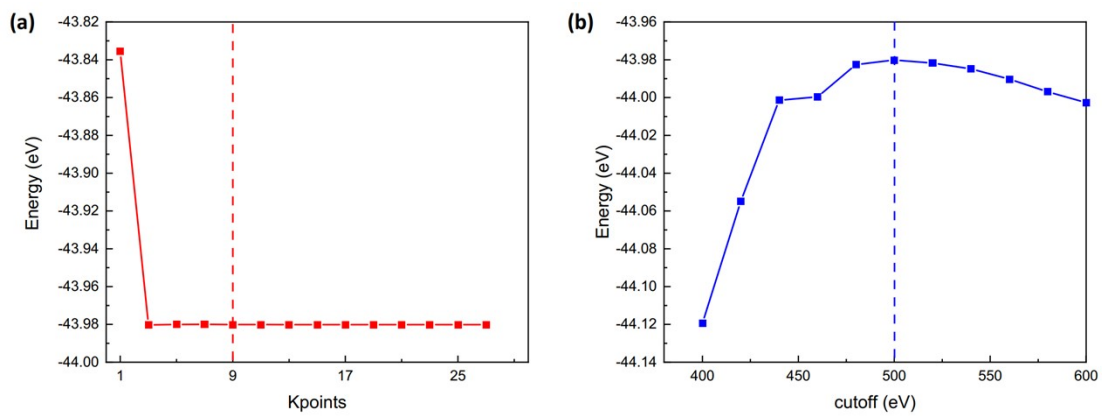
Fig. S6 Convergence test of total energy against the density of k-mesh and cutoff of selected plane wave.
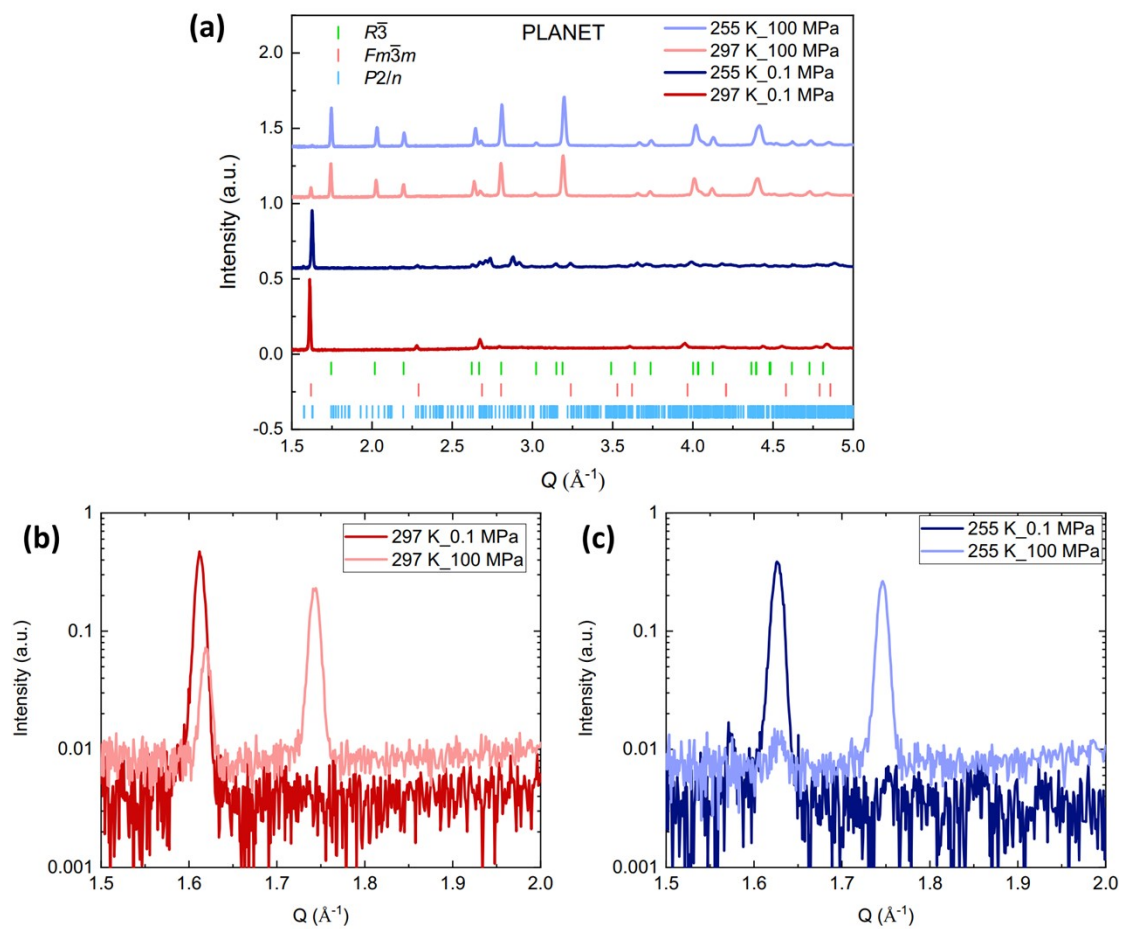
Fig. S7 The diffraction data of KPF_6 from PLANET at (297 K, 0.1 MPa), (297 K, 100 MPa), (255 K, 0.1 MPa) and (255 K, 100 MPa).
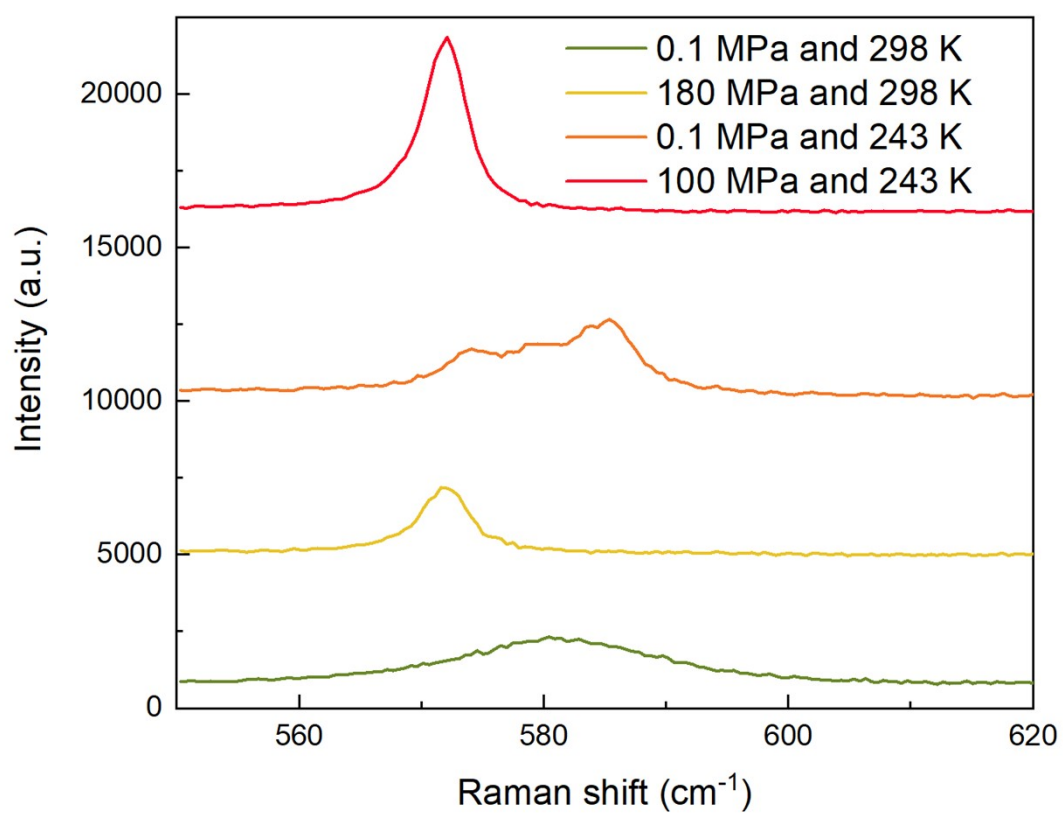
Fig. S8 Raman spectra at different temperatures and pressures around 580 cm^{-1} (Si oil is the pressure transmitting medium).

Table S1 Comparison of NPD and XRD lattice parameters.

Lattice Parameters	Method	a(Å)	b(Å)	c(Å)	β (degree)
Cubic	NPD (300 K)	7.78565(6)	7.78565(6)	7.78565(6)	90
	XRD (300 K)	7.7856(2)	7.7856(2)	7.7856(2)	90
monoclinic	NPD (240 K)	9.58160(12)	5.38325(7)	18.1248(2)	101.0960(15)
	XRD (250 K)	9.5725(6)	5.3827(3)	18.1556(12)	100.962(6)

Table S2 A comparison of the entropy changes of leading inorganic caloric materials.

Sample	$|dT_t/dP|$ (K GPa^{-1})	ΔP (MPa)	$|\Delta S_{P_0 \to P}|$ (J K^{-1} kg^{-1})	Ref.
AgI	140	250	60	23
$(NH_4)_2SO_4$	50	100	60	24
$Ni_{0.85}Fe_{0.15}S$	80	100	53	25
$LaFe_{11.33}Co_{0.47}Si_{1.2}$	10	200	8.7	26
$(MnNiSi)_{0.62}(FeCoGe)_{0.3}$ 8	80	270	74	27
NH_4I	810	40	71	4
$NdCu_3Fe_4O_{12}$	36.1	510	65.1	28
KPF_6	226	80	144	This work

Table S3 The lattice parameters under different pressures and temperatures.

Lattice Parameters	Pressure (MPa)	a(Å)	b(Å)	c(Å)	V(Å³)
	0.1	7.7920(2)	7.7920(2)	7.7920(2)	473.09(3)
297 K	282	7.18853(19)	7.18853(19)	7.1260(4)	318.90(2)
	792	7.1135(3)	7.1135(3)	7.0535(5)	309.10(3)
	0.1	9.5994(7)	5.3761(8)	18.160(2)	919.4(2)
255 K	241	7.1722(3)	7.1722(3)	7.1044(4)	316.49(3)
	758	7.1110(3)	7.1110(3)	7.0468(6)	308.59(3)

Table S4 The related parameters of Clausius–Clapeyron relation for phase transition.

Type	Temperature (K)	ΔV_t (m^3 kg^{-1})	dT_t/dP (K GPa^{-1})	ΔS_t (J kg^{-1} K^{-1})
monoclinic-to-cubic	250	0.37×10^{-5} $V(Fm\bar{3}m) - V(P2/n)$ (Fig S4)	78	47
rhombohedral-to-cubic	297	3.91×10^{-5} $(V_{0.1\,MPa} - V_{282\,MPa})$ (Table S3)	226	173

Table S5 The Raman peak position (~750 cm^{-1}) under different pressures and temperatures.

Temperature (K)	Pressure (MPa)	Raman shift (cm^{-1})	Energy transfer (meV)
293	0.1	751.75926(742)	93.15480
	400	753.58349(449)	93.38085
	1070	755.34173(423)	93.59873
243	0.1	751.96523(829)	93.18033
	340	753.51124(468)	93.37190
	1010	755.24885(468)	93.58722

References

1   B. Li, Y. Kawakita, S. Ohira-Kawamura, T. Sugahara, H. Wang, J. F. Wang, Y. N. Chen, S. I. Kawaguchi, S. Kawaguchi, K. Ohara, K. Li, D. H. Yu, R. Mole, T. Hattori, T. Kikuchi, S.-I. Yano, Z. Zhang, Z. Zhang, W. J. Ren, S. C. Lin, O. Sakata, K. Nakajima and Z. D. Zhang, *Nature*, 2019, **567**, 506.

2   K. Zhang, R. Q. Song, J. Qi, Z. Zhang, Z. Zhang, C. Y. Yu, K. Li, Z. D. Zhang and B. Li, *Adv. Funct. Mater.*, 2022, **32**, 2112622.

3   C. Y. Yu, J. Q. Huang, J. Qi, P. Liu, D. Li, T. Yang, Z. D. Zhang and B. Li, *APL Mater.*, 2022, **10**, 011109.

4   Q. Y. Ren, J. Qi, D. H. Yu, Z. Zhang, R. Q. Song, W. L. Song, B. Yuan, T. H. Wang, W. J. Ren, Z. D. Zhang, X. Tong and B. Li, *Nat. Commun.*, 2022, **13**, 2293.

5   V. Petříček, M. Dušek and L. Palatinus, *Z. Kristallog. - Cryst. Mater.*, 2014, **229**, 345.

6   J. Rodríguez-Carvajal, *Physica B: Condens. Matter*, 1993, **192**, 55.

7   J. Chen, L. Kang, H. L. Lu, P. Luo, F. W. Wang and L. H. He, *Physica B: Condens. Matter*, 2018, **551**, 370.

8   T. Hattori, A. Sano-Furukawa, H. Arima, K. Komatsu, A. Yamada, Y. Inamura, T. Nakatani, Y. Seto, T. Nagai, W. Utsumi, T. Iitaka, H. Kagi, Y. Katayama, T. Inoue, T. Otomo, K. Suzuya, T. Kamiyama, M. Arai and T. Yagi, *Nucl. Instrum. Methods Phys. Res. A*, 2015, **780**, 55.

9   T. Strässle, S. Klotz, K. Kunc, V. Pomjakushin and J. S. White, *Phys. Rev. B*, 2014, **90**, 014101.

10 C. M. Wu, G. Deng, J. S. Gardner, P. Vorderwisch, W. H. Li, S. Yano, J. C. Peng and E. Imamovic, *J. Instrum.*, 2016, **11**, P10009.

11 D. H. Yu, R. Mole, T. Noakes, S. Kennedy and R. Robinson, *J. Phys. Soc. Japan*, 2013, **82**, SA027.

12 D. H. Yu, R. A. Mole and G. J. Kearley, *EPJ Web of Conferences*, 2015, **83**, 03019.

13 D. Richard, M. Ferrand and G. J. Kearley, *J. Neutron Res.*, 1996, **4**, 33.

14 A. Furrer, J. F. Mesot, T. Strässle, *Neutron Scattering in Condensed Matter Physics* (World Scientific Publishing Co. Pte. Ltd, 2009).

15 H. G. Mao, J. Xu and P. M. Bell, *J. Geophys. Res. Solid Earth,* 1986, **91**, 4673.

16 G. Y. Shen, Y. B. Wang, A. Dewaele, C. Wu, D. E. Fratanduono, J. Eggert, S. Klotz, K. F. Dziubek, P. Loubeyre, O. V. Fat'yanov, P. D. Asimow, T. Mashimo and R. M. M.

Wentzcovitch, *High Press. Res.*, 2020, **40**, 299.

17   G. Kresse and J. Furthmüller, *Phys. Rev. B*, 1996, **54**, 11169.

18   P. E. Blöchl, *Phys. Rev. B*, 1994, **50**, 17953.

19   D. M. Ceperley and B. J. Alder, *Phys. Rev. Lett*, 1980, **45**, 566.

20   H. J. Monkhorst and J. D. Pack, *Phys. Rev. B*, 1976, **13**, 5188.

21   A. Togo, F. Oba and I. Tanaka, *Phys. Rev. B*, 2008, **78**, 134106.

22   S. Baroni, S. de Gironcoli, A. D. Corso and P. Giannozzi, *Rev. Mod. Phys.*, 2001, **73**, 515.

23   A. Aznar, P. Lloveras, M. Romanini, M. Barrio, J.-L. Tamarit, C. Cazorla, D. Errandonea, N. D. Mathur, A. Planes, X. Moya and L. Mañosa, *Nat. Commun.*, 2017, **8**, 1851.

24   P. Lloveras, E. Stern-Taulats, M. Barrio, J.-Ll. Tamarit, S. Crossley, W. Li, V. Pomjakushin, A. Planes, Ll. Mañosa, N. D. Mathur and X. Moya, *Nat. Commun.*, 2015, **6**, 8801.

25   J. C. Lin, P. Tong, X. K. Zhang, Z. C. Wang, Z. Zhang, B. Li, G. H. Zhong, J. Chen, Y. D. Wu, H. L. Lu, L. H. He, B. Bai, L. S. Lin, W. H. Song, Z. D. Zhang and Y. P. Sun, *Mater. Horizons*, 2020, **7**, 2690.

26   L. Mañosa, D. González-Alonso, A. Planes, M. Barrio, J.-L. Tamarit, I. S. Titov, M. Acet, A. Bhattacharyya and S. Majumdar, *Nat. Commun.*, 2011, **2**, 595.

27   T. Samanta, P. Lloveras, A. U. Saleheen, D. L. Lepkowski, E. Kramer, I. Dubenko, P. W. Adams, D. P. Young, M. Barrio, J. Ll. Tamarit, N. Ali, and S. Stadler, *Appl. Phys. Lett.*, 2018, **112**, 021907

28   Y. Kosugi, M. Goto, Z. H. Tan, A. Fujita, T. Saito, T. Kamiyama, W.-T. Chen, Y.-C. Chuang, H.-S. Sheu, D. Kan and Y. Shimakawa, *Adv. Funct. Mater.*, 2021, **31**, 2009476.